Supplementary Information (SI)

Drug release and solubility properties of two zeolitic metal-organic frameworks influenced by their hydrophobicity/hydrophilicity

Xiao-Hui Dong,[a] Zhi-Gang Li,[b] Dong-Yan Bian,[c] Tian-Meng Guo,[b] Zi-Ying Li,[b] Wei Li,[*b] Hongpeng He[*a]

[a] *Key Laboratory of Industrial Microbiology, Ministry of Education and Tianjin City, College of Biotechnology, Tianjin University of Science and Technology, Tianjin 300450, China.*

[b] *School of Materials Science and Engineering, Smart Sensing Interdisciplinary Science Center, Nankai University & TKL of Metal and Molecule Based Material Chemistry, Tianjin 300350, China.*

[c] *Department of Pharmacy, Tianjin Huanhu Hospital, Qixiangtai Road 122, Tianjin, China.*

The synthesis of ZIF-8-C:

330 mg of 2-methylimidazole was dissolved in 5 ml of methanol solvent. Simultaneously, 150 mg of zinc nitrate hexahydrate was dissolved in 5 ml of deionized water. Under stirring conditions, the zinc nitrate aqueous solution was added to the methanol solution of 2-methylimidazole. The solution gradually changed from transparent to a white suspension, indicating the formation of ZIF-8 particles. The resulting product was collected by centrifugation at 12,000 rpm for 30 min and washed three times with 20 ml of methanol each time to remove any unreacted reagents. Finally, the formed ZIF-8 was dried and stored in a vacuum drying oven at 50°C for 24 h.

The synthesis of MAF-7-C:

200 mg of 3-methyl-1,2,4-triazole was dissolved in 4.5 ml of deionized water as solution I. Simultaneously, 90 mg of zinc nitrate hexahydrate was dissolved in 4.5 ml of deionized water as solution II. Solution I and solution II were mixed, and 100 μL of 25% ammonia solution was added to the resulting mixture. The solution gradually changed from transparent to a white suspension. After stirring for 10 min, the product was collected by centrifugation at 10,000 rpm for 10 min. It was then washed three times with 20 ml of methanol each time to remove any unreacted reagents. The obtained MAF-7 product was dried and stored in a vacuum drying oven at 50°C for 24 h.

The synthesis of ZIF-8-A/MAF-7-A:

100 mg of ZIF-8/MAF-7 was added to a ball mill. Under room temperature conditions, ball milling was performed at 800 rpm for a duration of 10 min with a 5 min interval. The total ball milling time was 50 min.

Density Functional Theory Calculations

The first-principles calculations in this work were performed utilizing the Vienna *ab initio*

simulation package (VASP),[1,2] a total energy package based on plane-wave pseudopotential DFT. The exchange-correlation energy was described using the Perdew–Burke–Ernzerh generalized gradient approximation (GGA),[3] and the projector augmented wave (PAW) was adopted.[4] The Monkhorst–Pack type K point used in the calculations was 1×1×1 and the cut-off energy was set to 500 eV in all calculations. To account for dispersion effects, the zero damping DFT-D3 method of Grimme correlation was employed.[5] The total energy was converged to within 10^{-7} eV in all calculations, and residual forces on each atom were less than 0.01 eV/Å^{-1} in structure optimization calculations. The binding energy of Shikonin (SK) molecules with the framework is computed as: $E_b = E$ (MOF + SK) – E (MOF) – E (SK). Here, E (MOF + SK), E (MOF) and E (SK) are total energies of SK@MOF, individual MOF and SK, respectively.

Drug loading calculation

DLC (%) = (amount of loaded drug)/(amount of drug loaded MOFs)×100%

DLE (%) = (amount of loaded drug)/(total amount of feeding drug)×100%

To facilitate comparison, the conversions were performed. The drug loading capability (DLC) in SK-ZIF-8-C was determined to be 7.3 wt% and in SK-MAF-7-C was determined to be 2.1 wt%. This demonstrates 0.06 SK molecules per cage in ZIF-8 were encapsulated, 0.017 SK molecules per cage in MAF-7 were encapsulated respectively.

Table S1. Synthesis of SK-ZIF-8-C Nanoparticles.

	$Zn(NO_3)_2 \cdot 6H_2O$ Solvent(mL)	MIM+SK Solvent(mL)	SK(mg)	Reaction time(min)	DLC(%)	DLE(%)
1	MeOH, 5	MeOH, 5	5	60	8.7	14.3
2	MeOH, 5	MeOH, 5	10	60	19	8.3
3	H_2O, 5	MeOH, 10	5	60	2.3	18.1
4	H_2O, 5	MeOH, 5	5	60	6.2	61.8
5	H_2O, 5	MeOH, 5	5	10	6.3	63.4
6	H_2O, 10	MeOH, 5	5	10	7.3	81.1

Table S2. Synthesis of SK-MAF-7-C Nanoparticles.

	$Zn(NO_3)_2$ Solvent(mL)	MTZ Solvent(mL)	SK solvent	SK(mg)	Reaction time(min)	DLC(%)	DLE(%)
1	H_2O, 4	H_2O, 4	$NH_3 \cdot H_2O$	5	10	2.6	29.1
2	H_2O, 4	H_2O, 4	$NH_3 \cdot H_2O$	4	10	2.6	35.1
3	H_2O, 4	H_2O, 4	$NH_3 \cdot H_2O$	3	10	2.5	41.3
4	H_2O, 4	H_2O, 4	$NH_3 \cdot H_2O$	2	10	2.1	53.4

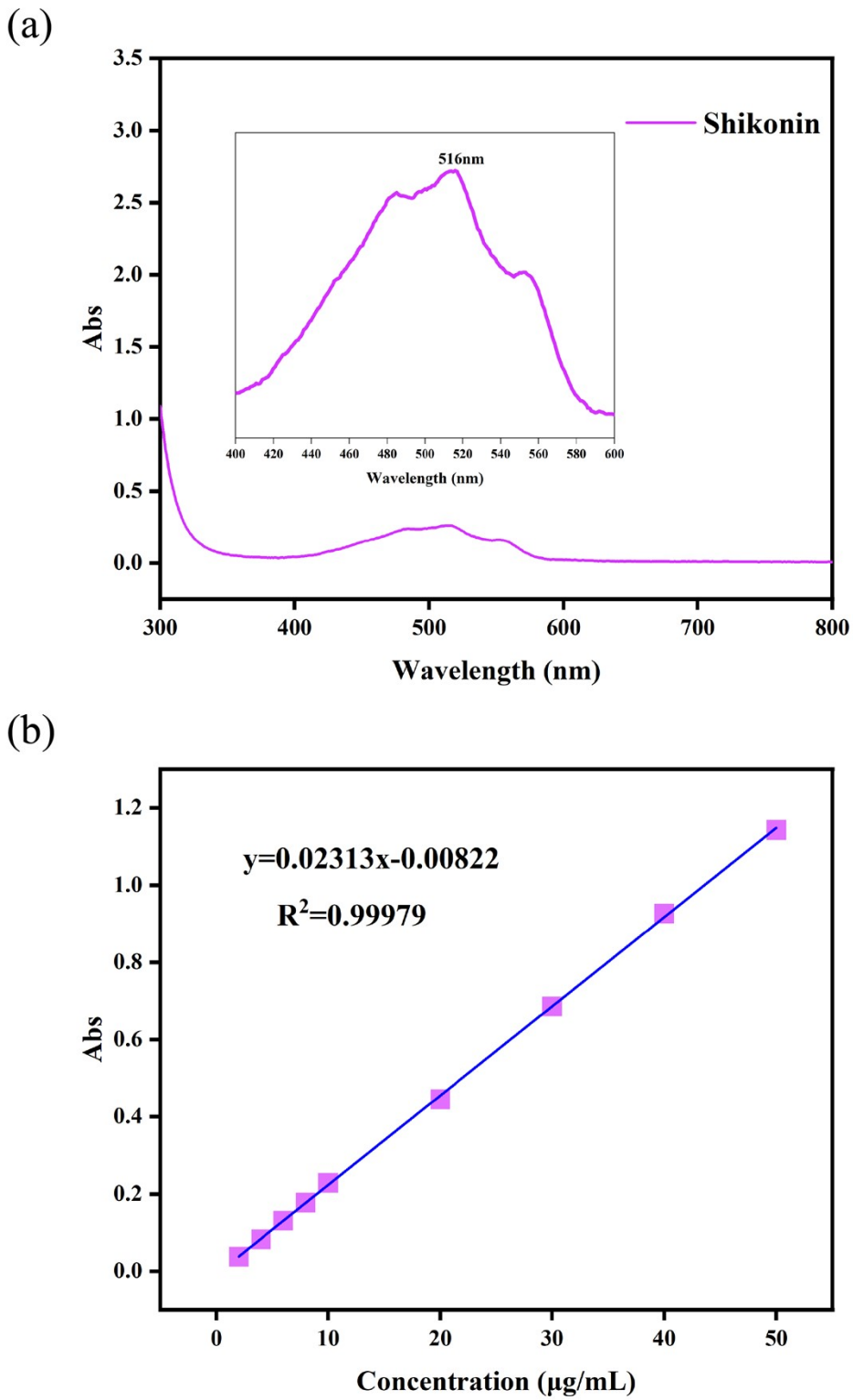

Fig. S1. Full wavelength scan of the UV-vis absorption spectrum of SK in methanol solvent (a). UV-Vis absorption spectrum shows that SK exhibits the maximum absorption at 516 nm. The linear relationship between the concentration of SK and absorption intensity in methanol (b). The UV-vis absorbance of SK methanol solutions at different concentrations was measured using a 1 cm quartz cell to determine the standard curves for SK. The fitted linear relationship between absorption intensity at 516 nm and SK concentration allows for reliable evaluation of SK loading efficiency in composites.

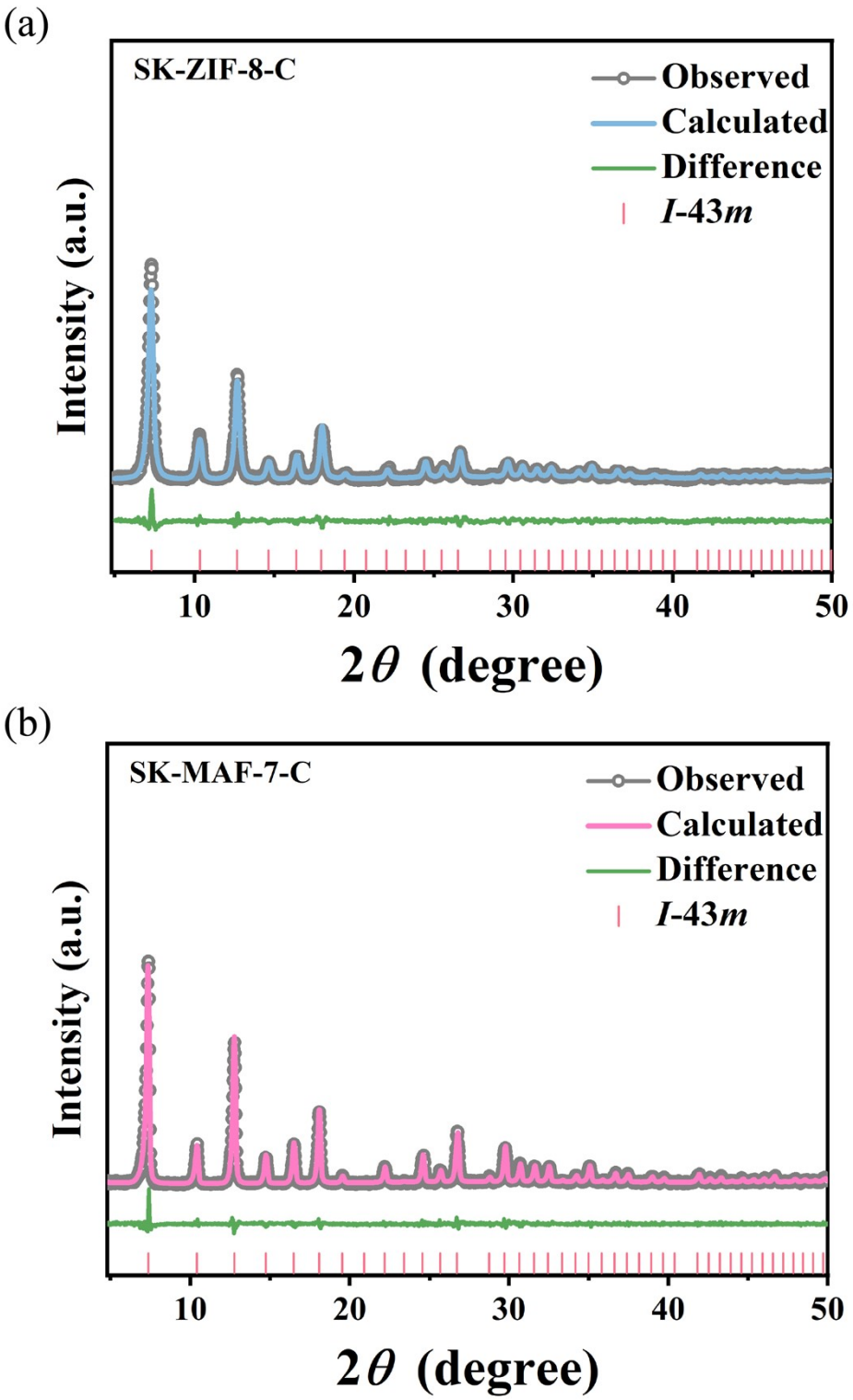

Fig. S2 PXRD patterns of SK-ZIF-8-C (a) and SK-MAF-7-C (b) after refinement. PXRD utilizing Cu Kα radiation (λ = 1.540593 Å), the PXRD patterns of the specimens were recorded on a Rigaku powder diffractometer that scanned at 5 degrees per minute, with a step size of 0.02. Le Bail whole profile fitting was carried out using the Total Pattern Solution (TOPAS) software.

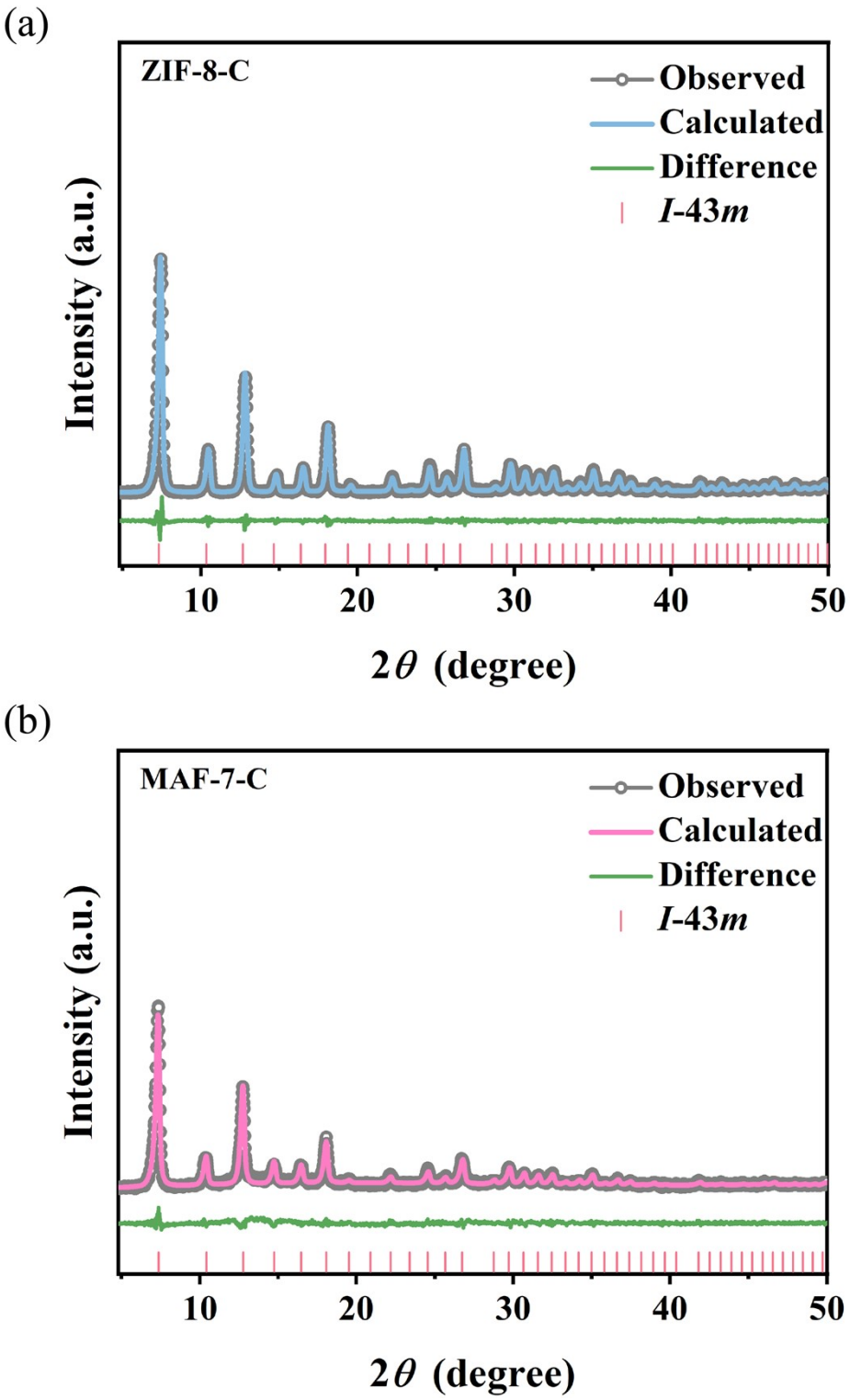

Fig. S3 PXRD patterns of ZIF-8-C (a) and MAF-7-C (b) after refinement.

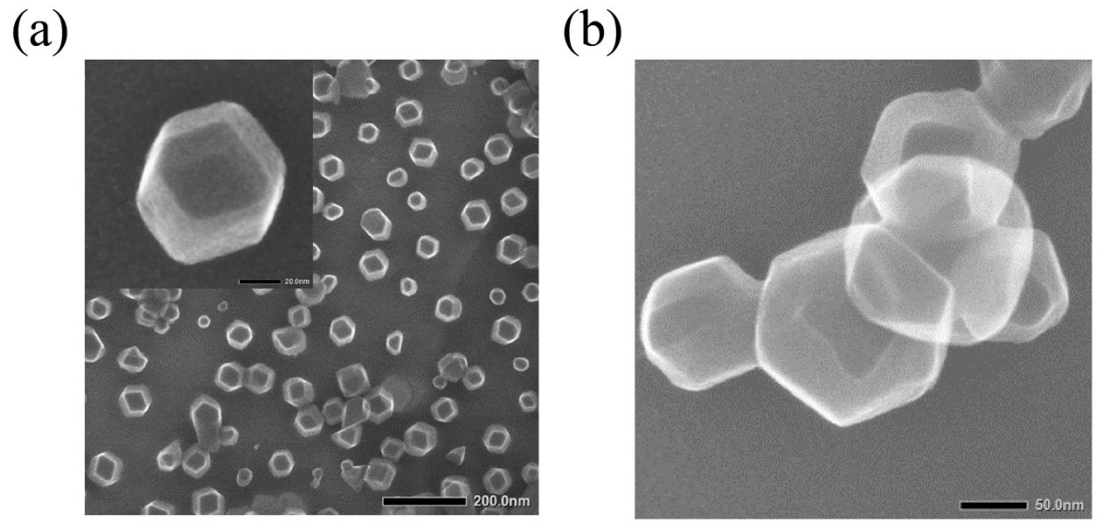

Fig. S4 TEM images for ZIF-8-C (a) and MAF-7-C (b). TEM analysis was carried out in JEM-2800.

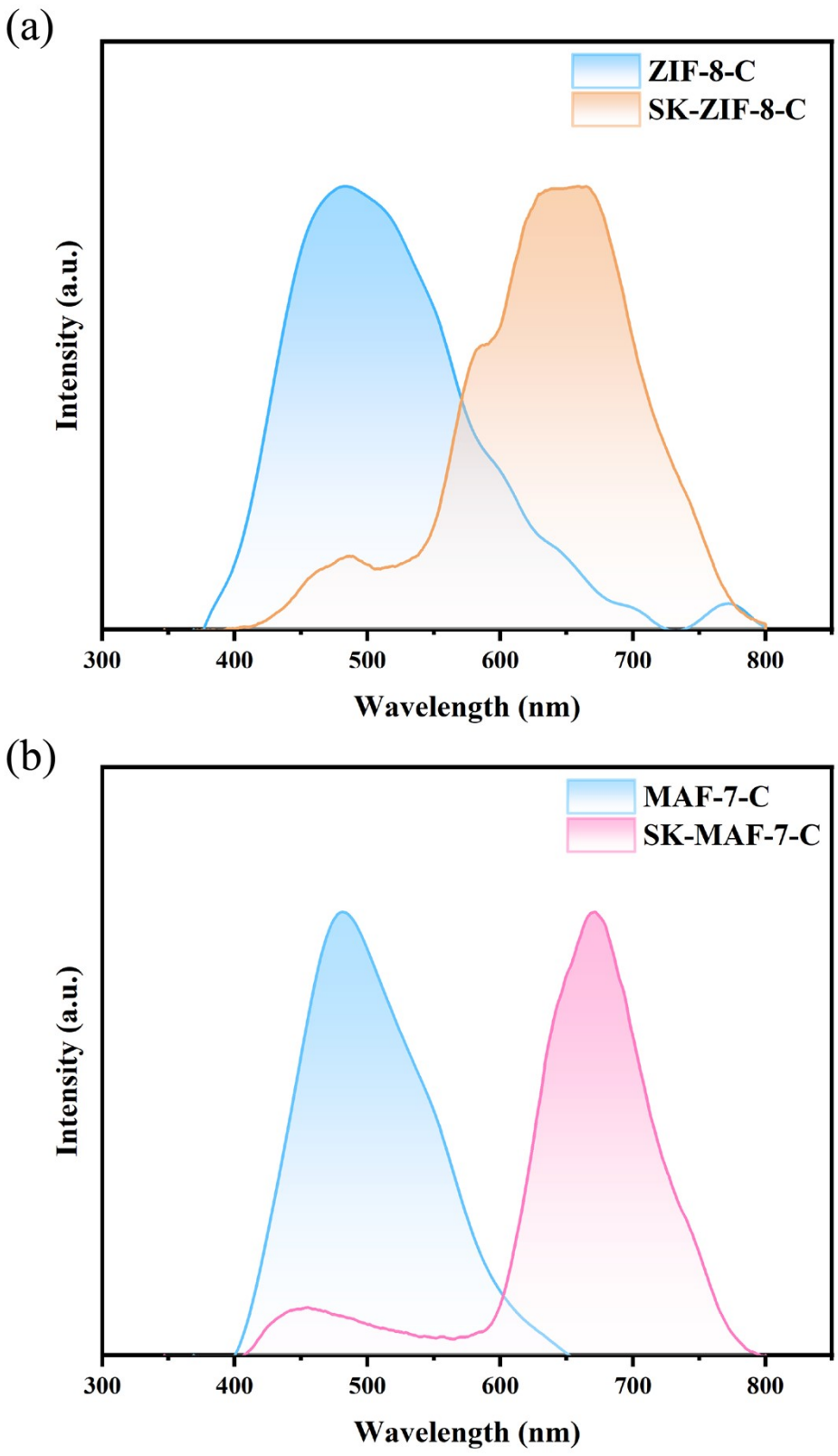

Fig. S5 The PL spectra of ZIF-8-C and SK-ZIF-8-C (a), MAF-7-C and SK-MAF-7-C (b).

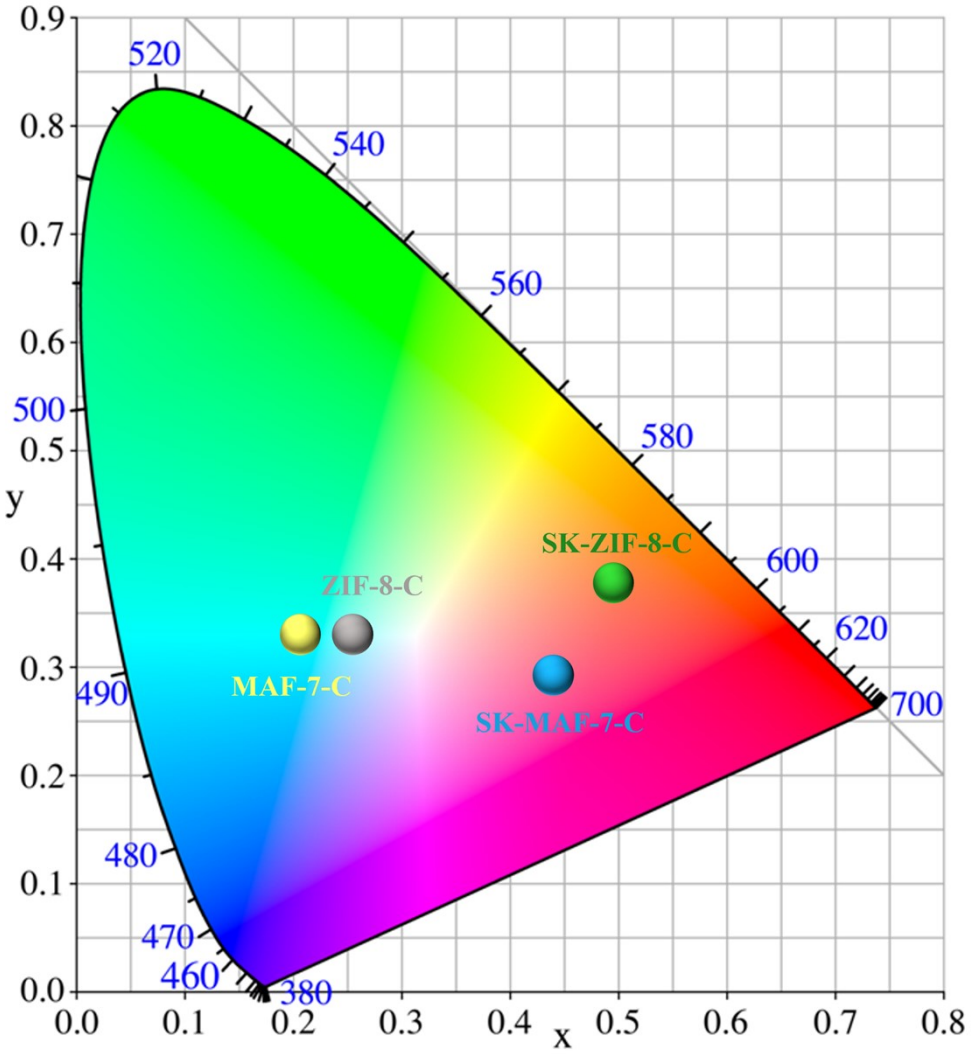

Fig. S6 Selected coordinates of PL emission on CIE 1931 color space for ZIF-8-C, MAF-7-C, SK-ZIF-8-C, and SK-MAF7-C, respectively.

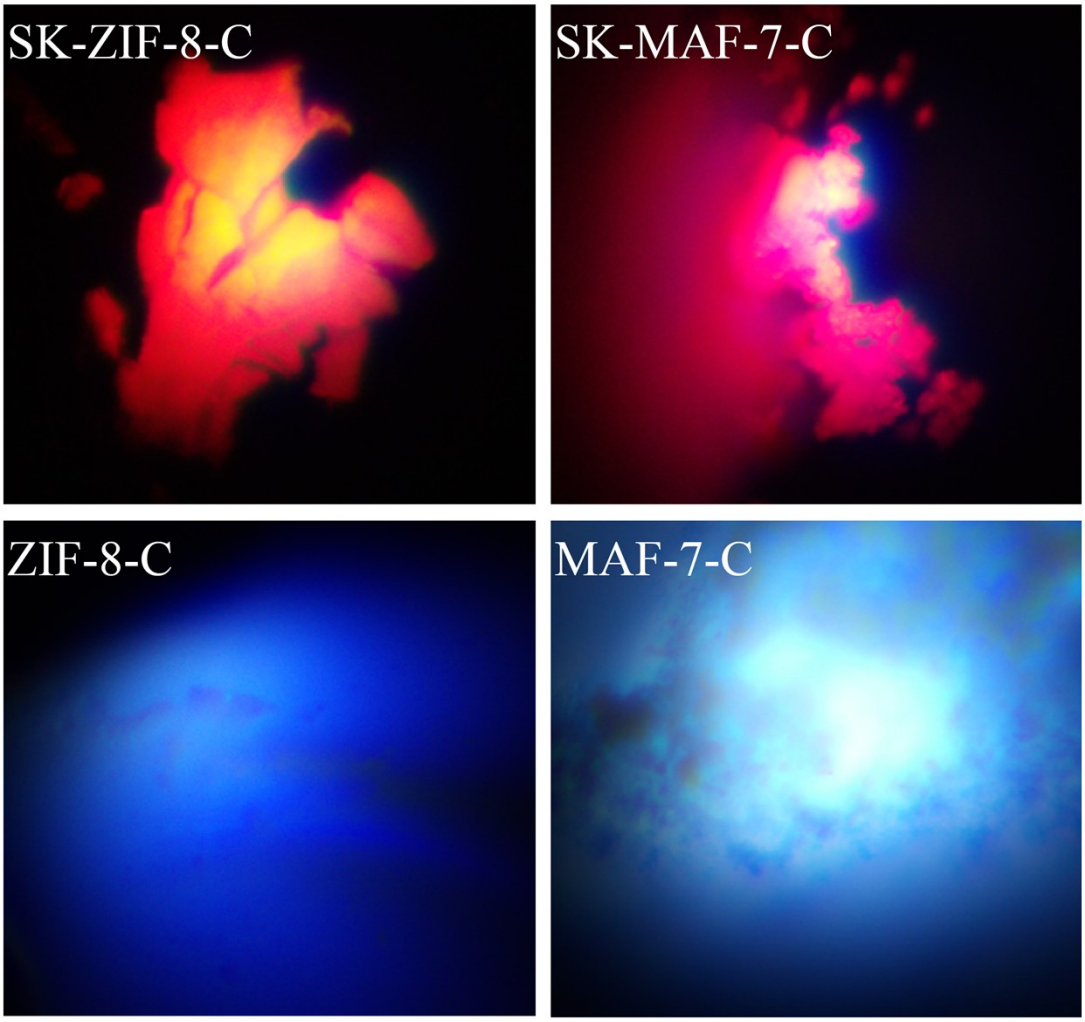

Fig. S7 Fluorescence images of SK-ZIF-8-C, SK-MAF-7-C, ZIF-8-C, and MAF-7-C.

Fig. S8 Shikonin shows red fluorescence in dilute methanol solution (left) but no fluorescence in aggregates (right).

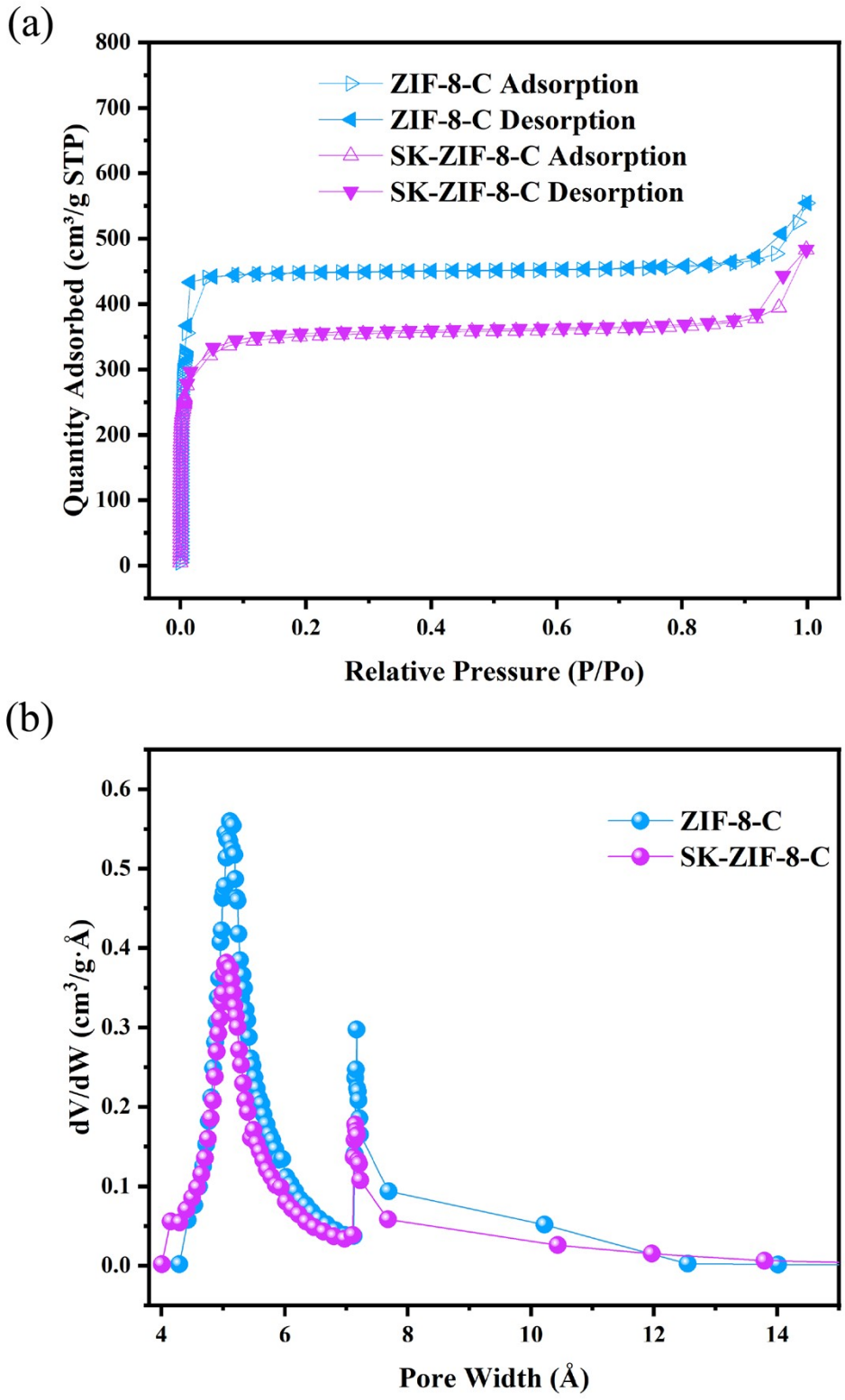

Fig. S9 (a)77 K N_2 adsorption (filled symbol) and desorption (open symbol) isotherms for ZIF-8-C (blue) and SK-ZIF-8-C (purple). Gas adsorption isotherm measurements are carried out on the ASAP 2460 surface area and porosity analyzer. (b) The corresponding pore size distribution of ZIF-8-C (blue) and SK-ZIF-8-C (purple) was calculated by Horvath-Kawazoe method.

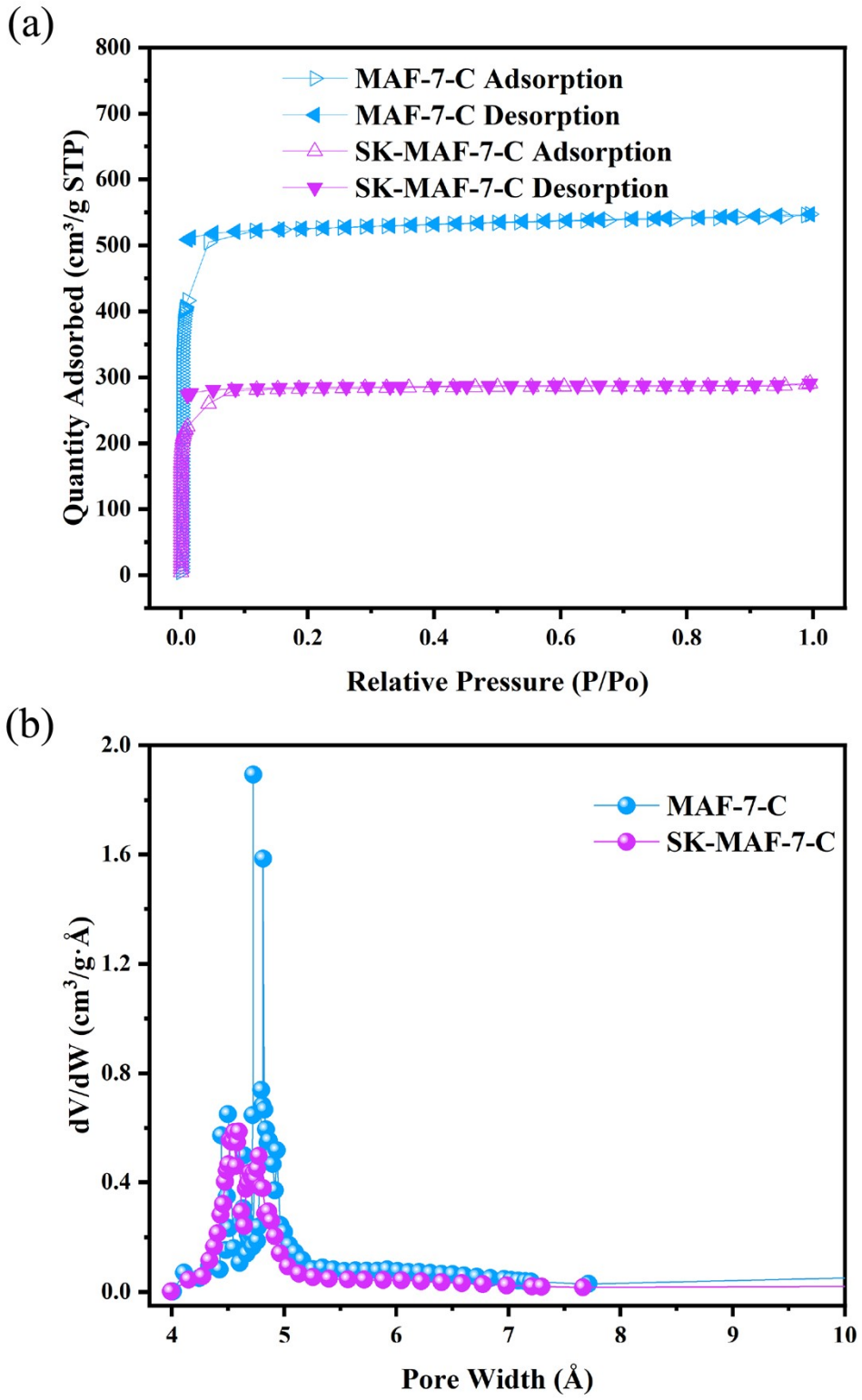

Fig. S10 (a)77 K N_2 adsorption (filled symbol) and desorption (open symbol) isotherms for MAF-7-C (blue) and SK-MAF-7-C (purple). (b) The corresponding pore size distribution of MAF-7-C (blue) and SK-MAF-7-C (purple) was calculated by Horvath-Kawazoe method.

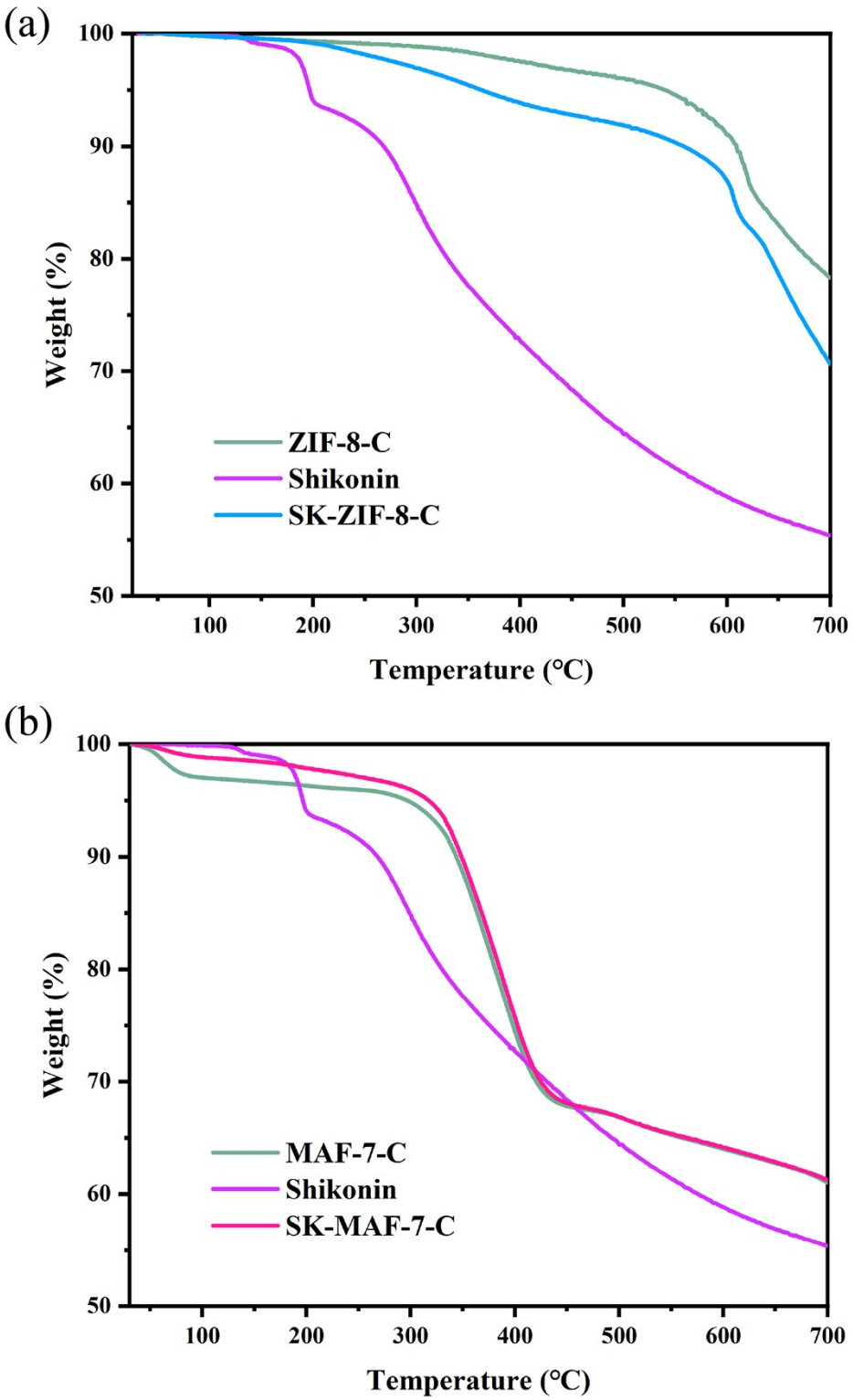

Fig. S11 TGA curves showing the weight loss and decomposition for ZIF-8-C, SK-ZIF-8-C, and SK (a). TGA curves of MAF-7-C, SK-MAF-7-C, and SK (b). The amount of SK encapsulated within different materials was assessed by TGA. TGA was performed using NETZSCH TG 209 F1 Libra instrument. The program used was under Nitrogen air flow from 30 ºC to 700ºC with a heating ramp of 10 ºC/min.

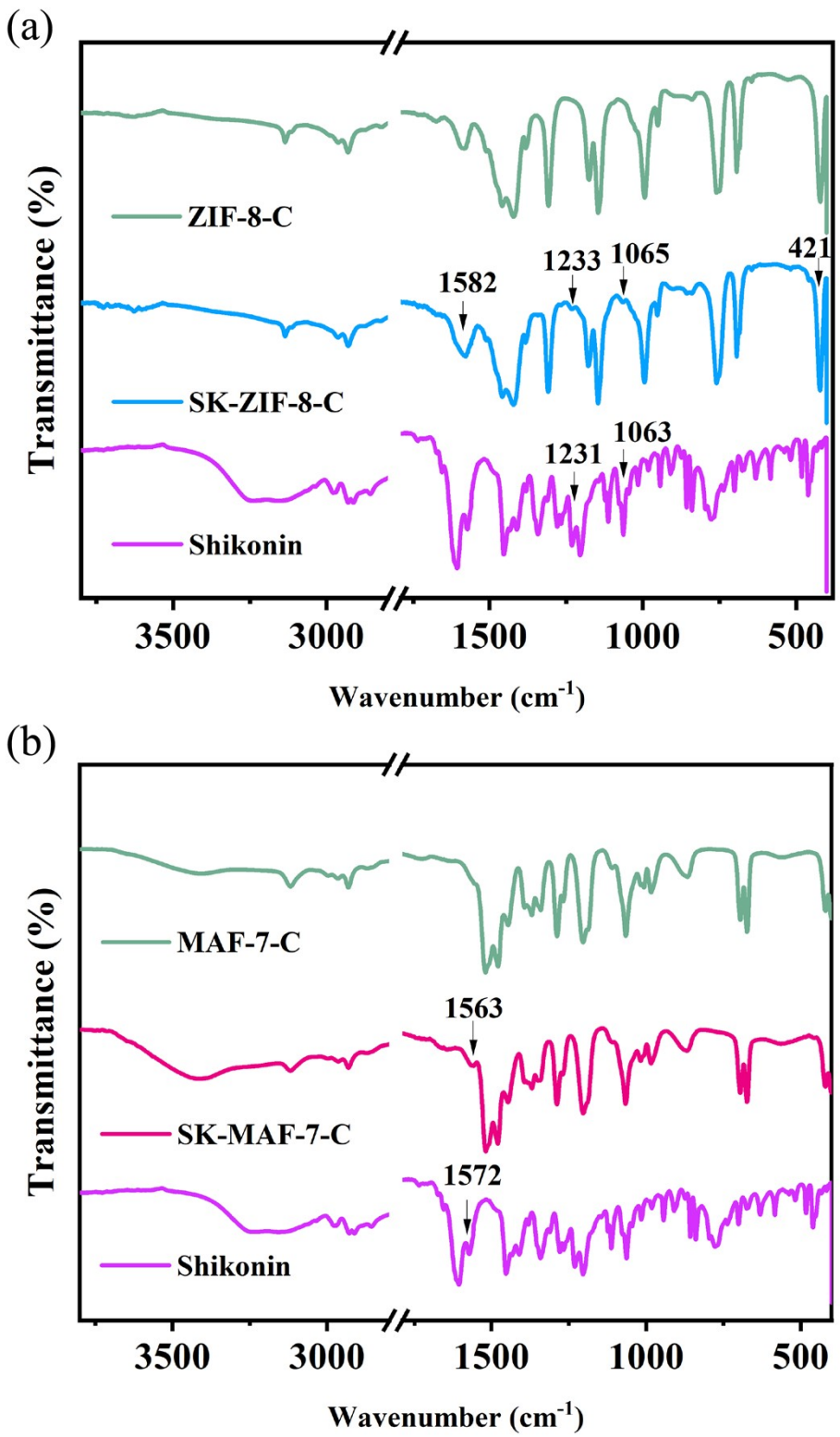

Fig. S12 IR spectra of SK-ZIF-8-C composite compared to ZIF-8-C and SK (a). IR spectra of SK-MAF-7-C composite compared to MAF-7-C and SK (b). Fourier-transform infrared (FT-IR) spectra were acquired using a Thermo Scientific Nicolet iS20 spectrometer equipped with an attenuated total reflectance (ATR) accessory featuring a diamond window. The spectra were collected in the wavenumber range of ν 400–4000 cm^{-1}, with a resolution of 4 cm^{-1} and an average of 32 scans.

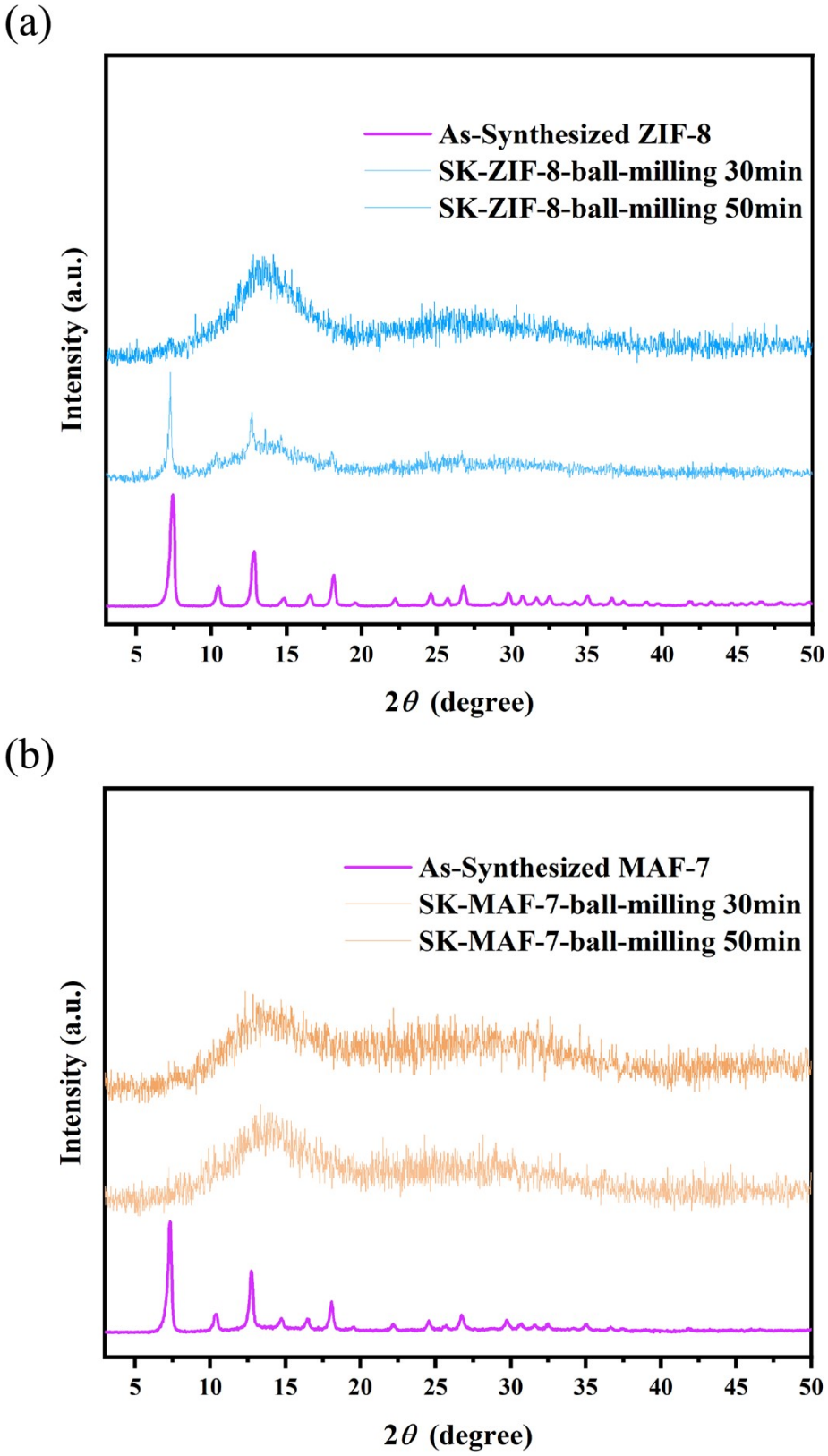

Fig. S13 PXRD patterns of SK-ZIF-8 (a) and SK-MAF-7 (b) after ball milling.

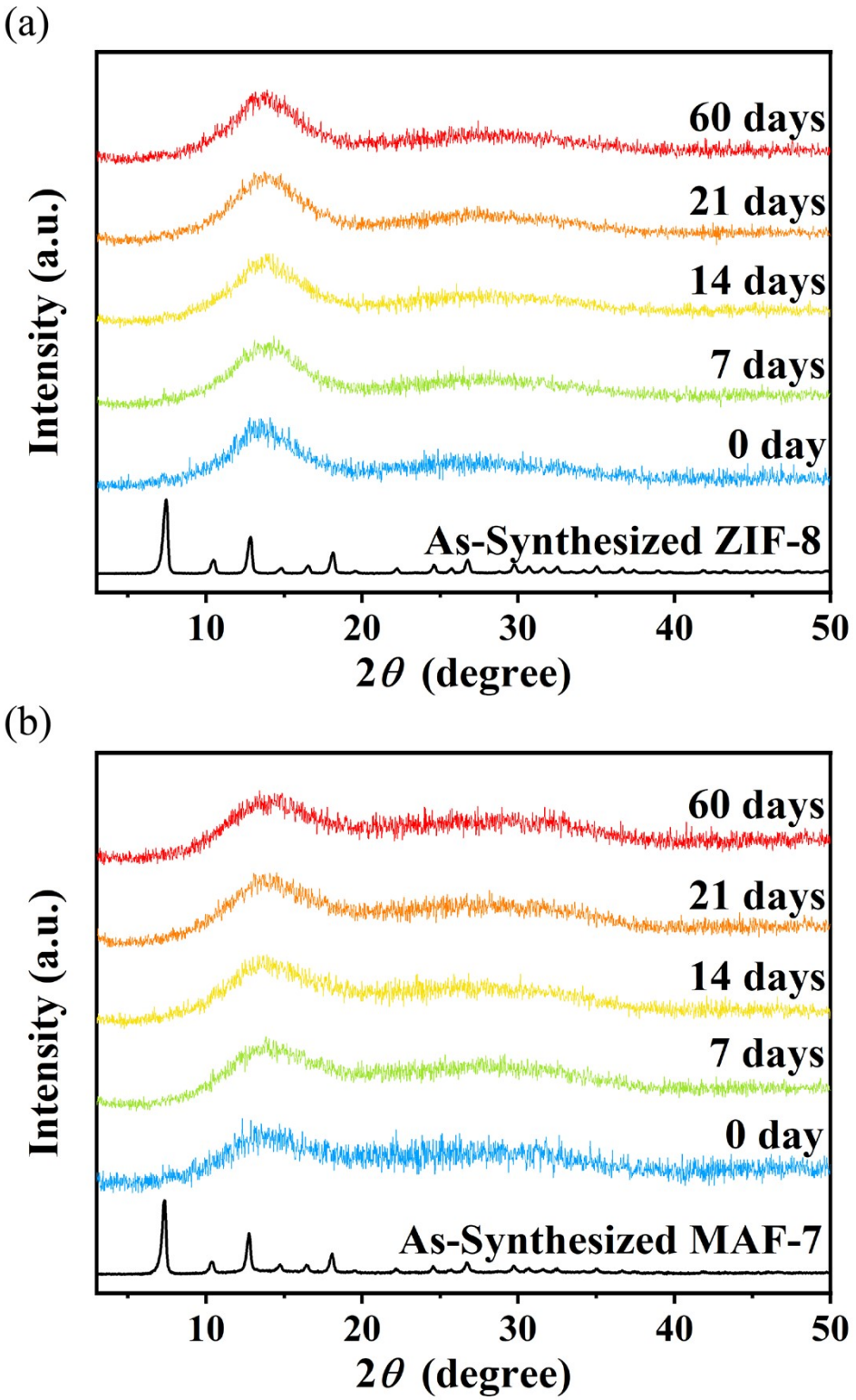

Fig. S14 PXRD patterns of SK-ZIF-8-A (a) and SK-MAF-7-A (b) co-amorphous system after 0, 7, 14, 21 and 60 days.

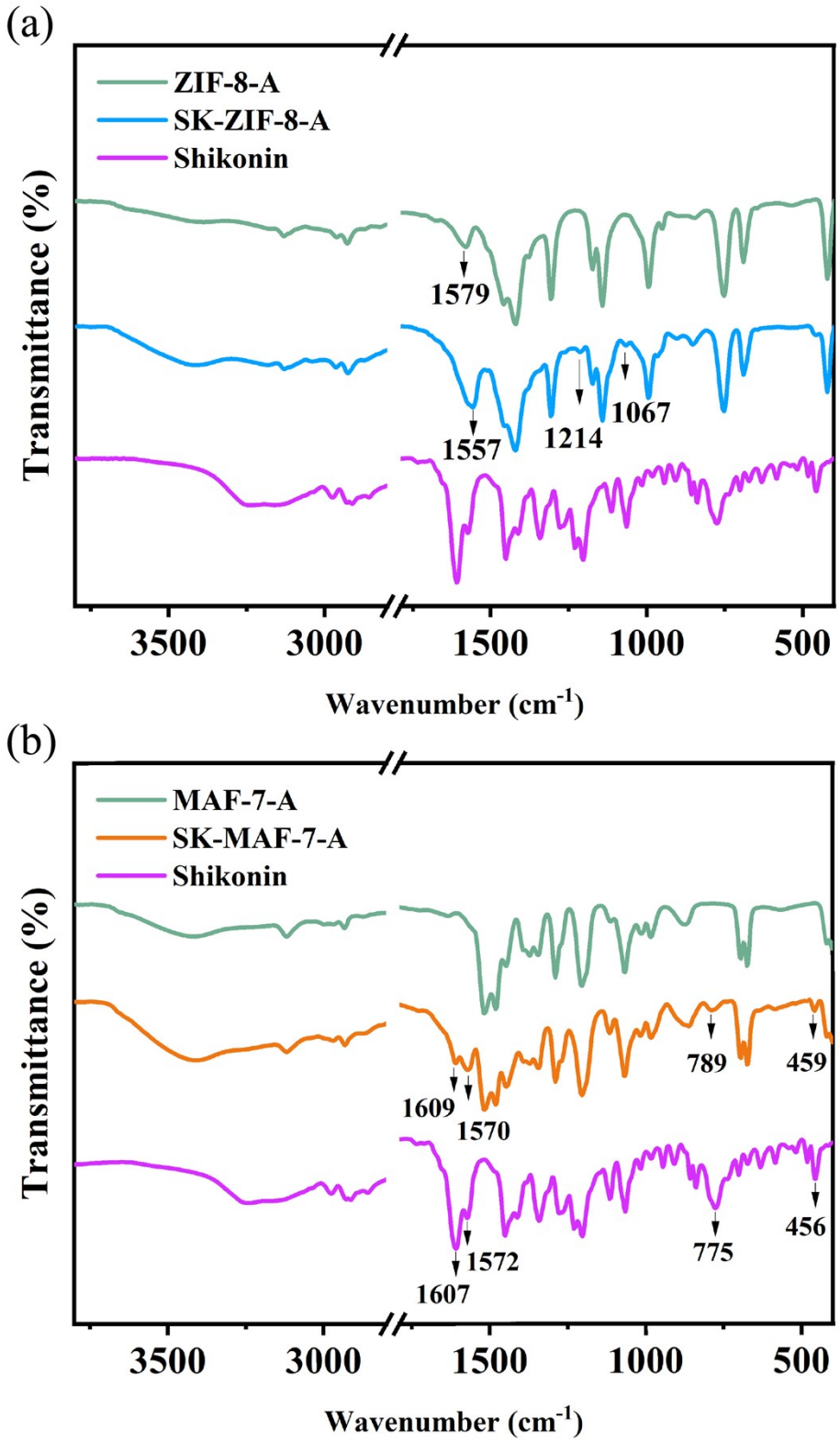

Fig. S15 IR spectra of co-amorphous SK-ZIF-8-A compared to SK and amorphous ZIF-8 (a). IR spectra of co-amorphous SK-MAF-7-A compared to SK and amorphous MAF-7 (b).

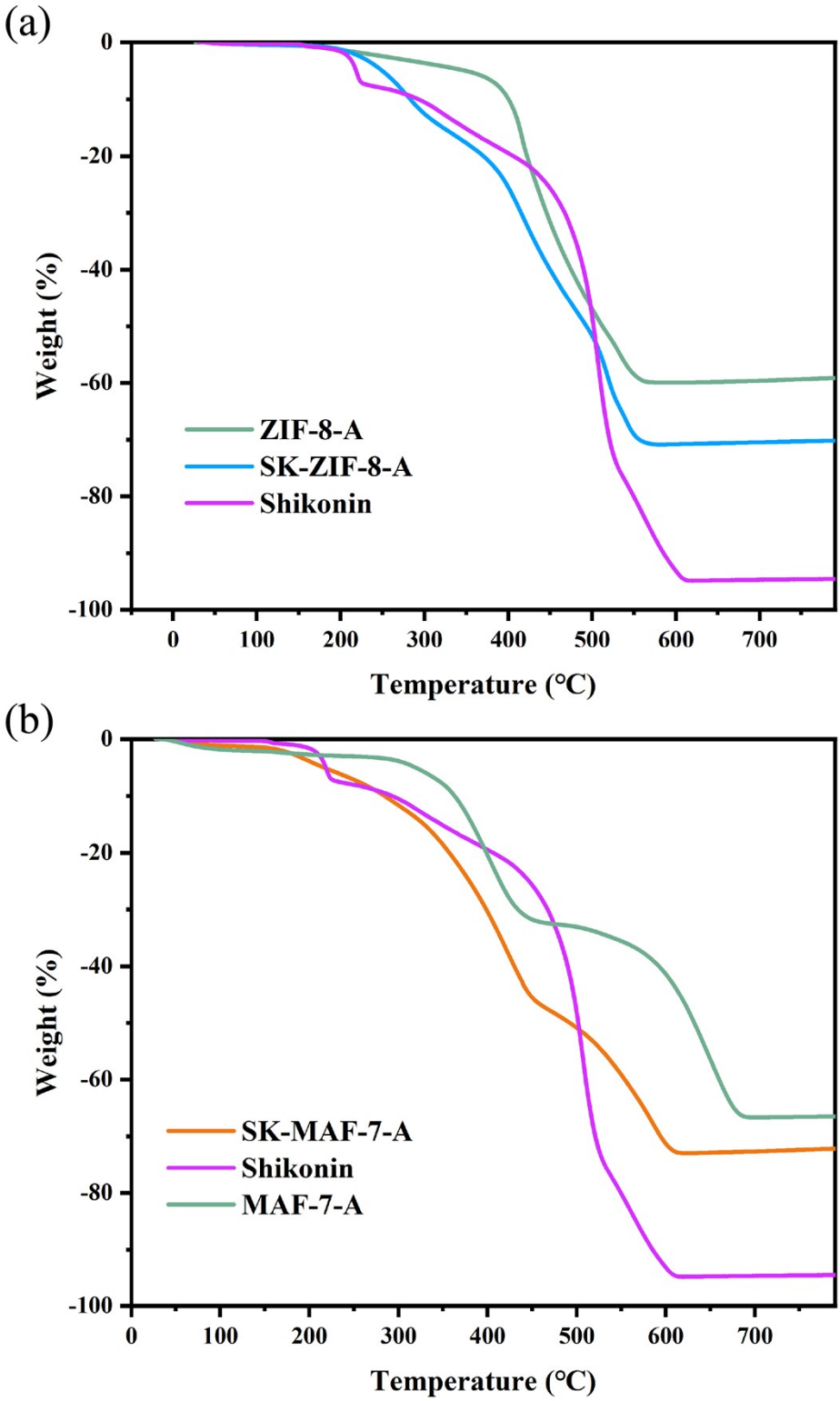

Fig. S16 TGA curves showing the weight loss and decomposition for ZIF-8-A, SK-ZIF-8-A, and SK (a). TGA curves of MAF-7-A, SK-MAF-7-A, and SK (b).

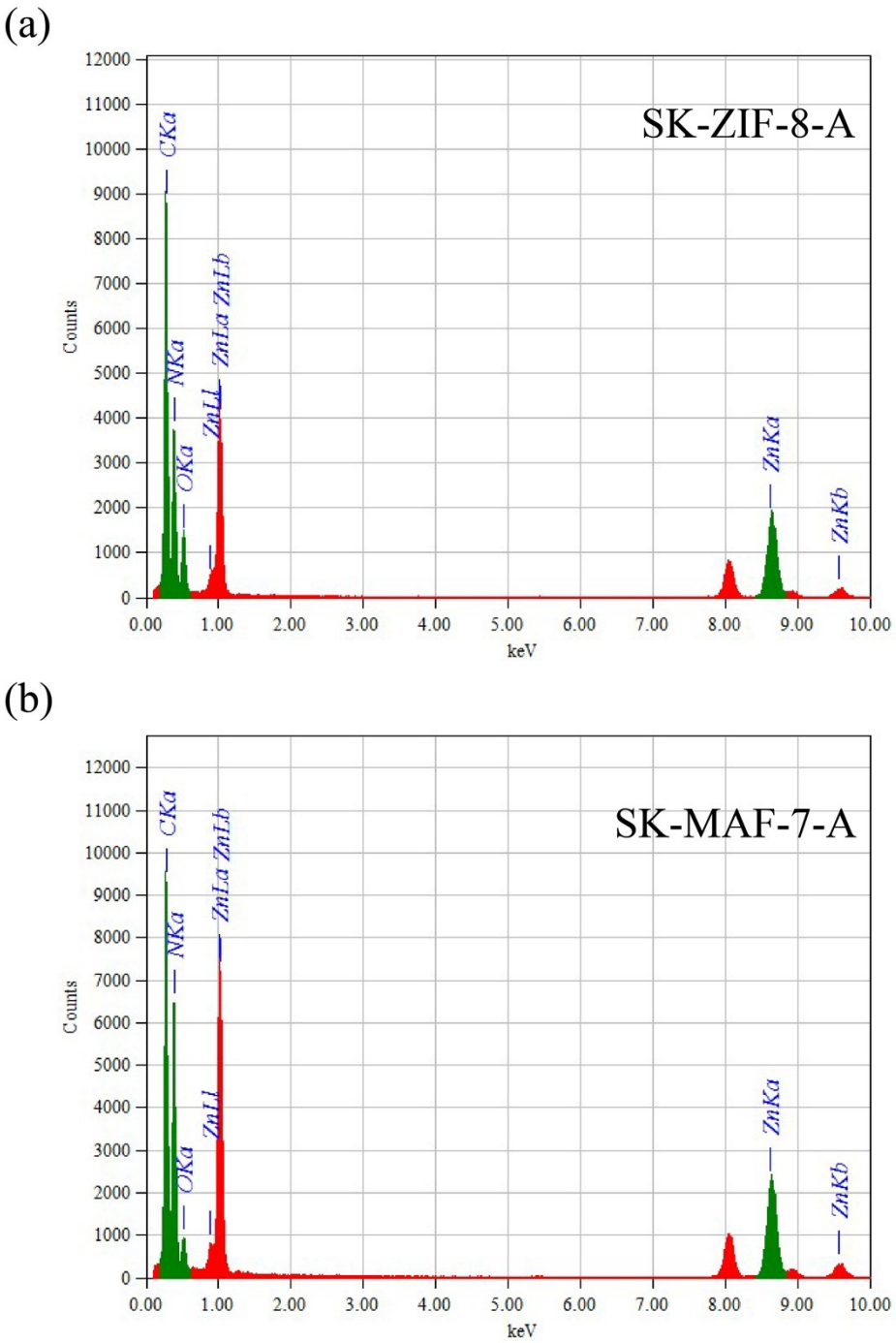

Fig. S17 EDS spectra of SK-ZIF-8-A (a) and SK-MAF-7-A (b).

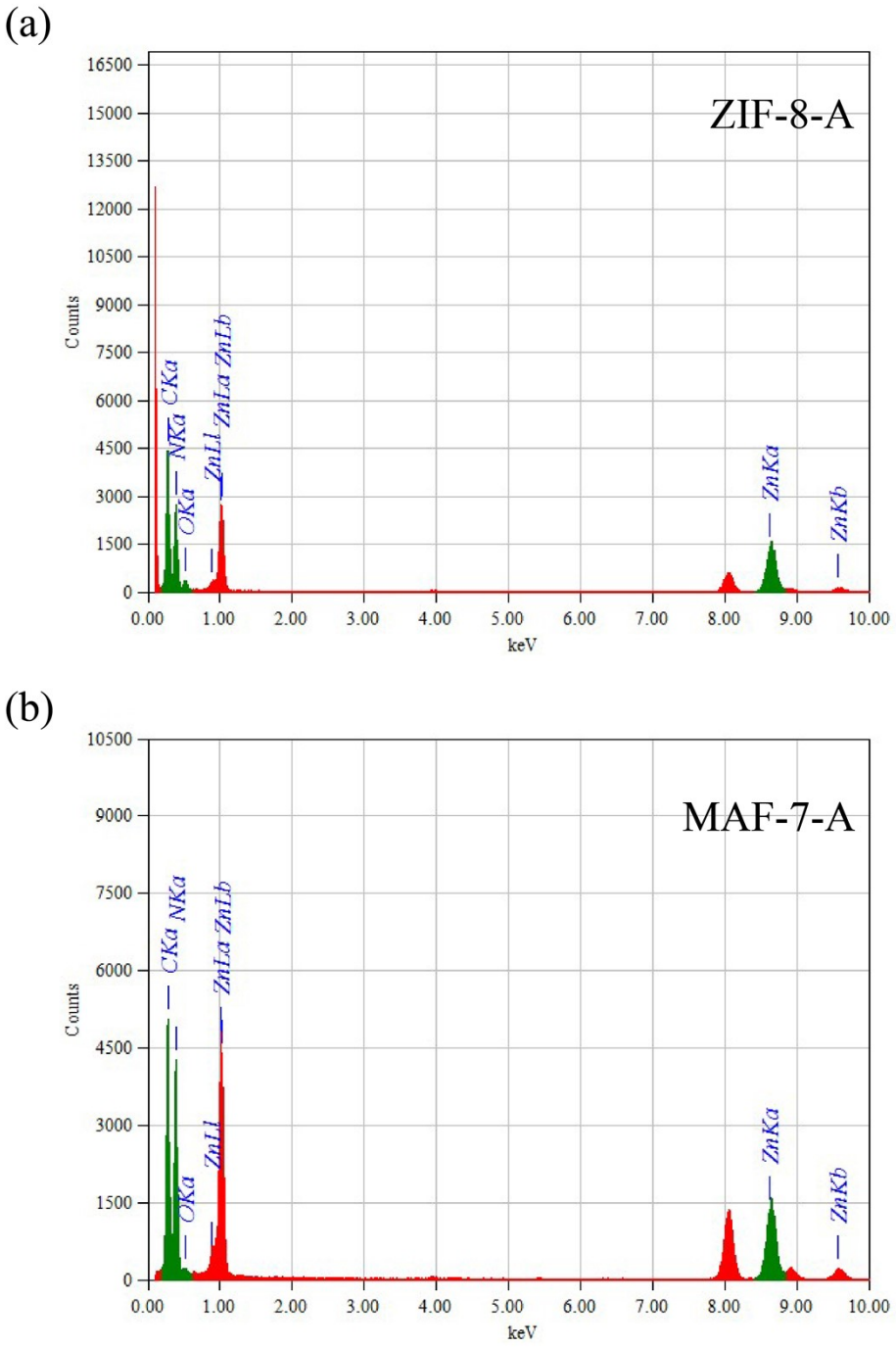

Fig. S18 EDS spectra of ZIF-8-A (a) and MAF-7-A (b).

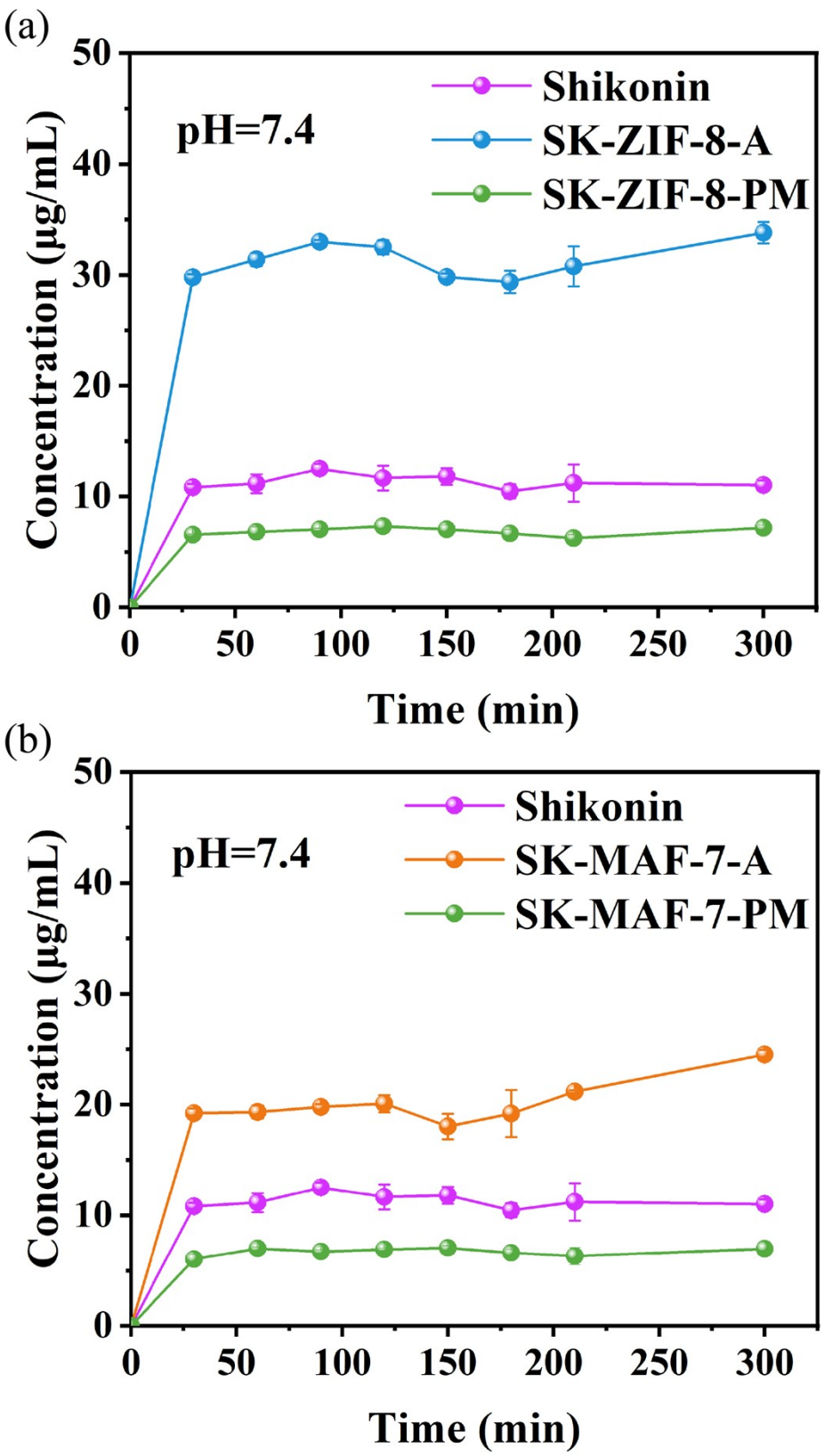

Fig. S19 Supersaturated dissolution curves of co-amorphous SK-ZIF-8-A and physical mixture SK-ZIF-8-PM compared to SK at pH7.4 PBS buffer solution (a). Supersaturated dissolution curves of co-amorphous SK-MAF-7-A and physical mixture SK-MAF-7-PM compared to SK at pH7.4 PBS buffer solution (b).

References

1 G. Kresse and J. Furthmüller, Efficient iterative schemes for ab initio total-energy calculations using a plane-wave basis set, *Phys. Rev. B*, 1996, **54**, 11169–11186.

2 G. Kresse and J. Furthmüller, Efficiency of ab-initio total energy calculations for metals and semiconductors using a plane-wave basis set, *Comput. Mater. Sci.*, 1996, **6**, 15–50.

3 J. P. Perdew, K. Burke and M. Ernzerhof, Generalized gradient approximation made simple [Phys. Rev. Lett. 77, 3865 (1996)], *Phys. Rev. Lett.*, 1997, **78**, 1396–1396.

4 P. E. Blöchl, Projector augmented-wave method, *Phys. Rev. B*, 1994, **50**, 17953–17979.

5 S. Grimme, S. Ehrlich and L. Goerigk, Effect of the damping function in dispersion corrected density functional theory, *J. Comput. Chem.*, 2011, **32**, 1456–1465.